J. Fluid Mech. (2004), *vol.* 498, *pp.* 183–203.
DOI: 10.1017/S0022112003006888 Printed in the United Kingdom

The settling and dispersion of small dense particles by spherical vortices

By I. EAMES[1] AND M. A. GILBERTSON[2]

[1]Departments of Mechanical Engineering and Mathematics, University College London, Torrington Place, London WC1E 7JE, UK

[2]Department of Mechanical Engineering, University of Bristol, University Walk, Bristol BS8 1TR, UK

(Received 20 May 2003 and in revised form 19 August 2003)

The gravitational settling of small dense particles (with fall speed v_T, response time τ_p) past an isolated spherical vortex (radius a, speed U) or a random distribution of spherical vortices translating vertical upwards, is examined. As particles sediment past a vortex, they are permanently displaced vertically and laterally a distance X and Y, respectively. The bulk settling properties of the particles are expressed in terms of the weighted moments of displacement, denoted by D_p, M_{xx}, M_{yy} and corresponding to the integral of X, $X^2/2$, $Y^2/2$, respectively over the particle sheet. When the particle Stokes number $St = U\tau_p/a \to 0$, the particles are inertialess. Particles starting outside the vortex are excluded from a spherical shadow region when $v_T/U > 3/2$. When $v_T/U < 3/2$, particles passing close to the particle stagnation points (in the frame moving with the vortex) are held up for a long time relative to particles far from the vortex, but are not displaced laterally. In an unbounded flow, the particle drift volume, D_p, is calculated using a geometrical argument, $M_{xx} = 25U^2\pi a^4/8(v_T + U)^2$, and $M_{yy} = 0$. As $v_T/U \to 0$, the results of Darwin (1953) are recovered. Results for finite values of St are calculated numerically. The effect of inertia is shown to substantially increase the particle residence time near the vortex because particles overshoot the particle stagnation point, and there is a shadow region within and behind the vortex. D_p, M_{xx}, and M_{yy} all substantially increase with the particle Stokes number. These results are applied to calculate the bulk settling velocity and the dispersivity of particles sedimenting through a random distribution of vortices translating vertically in a bounded flow. This is done by combining information of the particle displacements with a statistical model of their encounter with a vortex. Inertialess particles ($St = 0$) do not experience the upwards flow within the vortex and the fractional increase in fall speed is proportional to the volume of the shadow region. As St increases, particles overshoot the particle stagnation point, increasing their residence time and so decreasing the bulk settling fall speed. Particle inertia significantly increases the vertical dispersivity of dense particles compared to fluid particles, but for high v_T, particles disperse vertically more slowly than fluid particles.

1. Introduction

Coherent flow structures and turbulence stir up and disperse dense particles in a wide range of chemical engineering and environmental flows. In some problems the coherent structures are deliberately created by the container geometry or the forcing of the flow (e.g. oscillatory flow and baffled reactors or stirred tanks (Roberts & Mackley 1996)), in others they are spontaneously generated by an intrinsic instability

of the system (e.g. bubbling gas bubbles in fluidized beds (Rowe 1962)), or are generated in three-dimensional flows by an energy cascade to smaller length scales (Vincent & Meneguzzi 1994). These coherent vortical structures generate regions of significant strain and are the primary agents for dispersing and mixing particles.

Progress has be made in understanding the bulk settling speed and dispersion of dense particles in complex structured flows by calculating Lagrangian information of individual particle dynamics so that closures for dilute particle-laden flows can be developed and fed into Eulerian models of dispersed two-phase flows. The starting point for this approach is calculation of the Lagrangian motion of a single particle relative to a vortex. This has been previously exploited successfully by Dávila & Hunt (2001) for small particles in vortices, and by Batchelor & Nitsche (1994) and Gilbertson & Yates (1995) for understanding bubbles in gas-fluidized beds. Information about the individual particle trajectories can then be statistically averaged to obtain bulk properties for the flow field (see Eames & Bush 1999; Dávila & Hunt 2001).

One of the advantages of Lagrangian models is that they enable bulk properties to be connected to the individual particle dynamics. For example, a fundamental problem for dilute particle-laden flows is whether particles sediment faster or slower in a turbulent flow. The vast literature on particles sedimenting in a turbulent field has given slightly contradictory answers to this question. This has arisen in part from slightly different definitions of an 'average' fall velocity and exactly how this is calculated. Dávila & Hunt (2001) described two different approaches to the averaging: an ensemble spatial average of the particle velocity field, and one based on an average particle residence time. In an effort to quantify the bulk settling velocity of particles in a turbulent flow, Dávila & Hunt (2001) used a Rankine vortex to represent the intense vortical tubes observed in direct numerical simulations (Vincent & Meneguzzi 1994) and then examined how initially horizontal sheets of particles are deformed as they sediment past it. By averaging over the collective effect of a large number of such vortices, Dávila & Hunt (2001) showed how the bulk settling velocity critically depends on the particle Froude number, which controls whether particles are pushed to the faster moving side of the vortex (which increases the settling velocity – see Maxey 1987) or are hindered as they overshoot a particle stagnation point (which reduces the settling velocity). Dávila & Hunt (2001) were able to capture this range of phenomena in a single Lagrangian model because they accounted for the significant deviation of the particle trajectory from the vertical owing to the occurrence of particle stagnation points. Their conclusions are supported by the experimental results of Srdic (1999).

Another fundamental problem concerning turbulent dilute particle-laden flows is whether particles disperse faster or slower than fluid particles. The particles' dispersivity is characterized by a highly anistropic tensor, $\mathscr{D}^{(p)}$, even when the forcing flow is homogeneous and the fluid dispersivity tensor, $\mathscr{D}^{(f)}$, is isotropic (Csanady 1963). Most studies draw concepts directly from the turbulence literature, where the dispersivity is expressed in terms of the Lagrangian velocity autocorrelation function (Taylor 1928). Soo (1967) developed a statistical description of aerosol particles (in the absence of buoyancy forces) forced by a random flow and showed how small particles disperse at the same rate as fluid particles. This argument is now known to be incorrect because it neglected spatial variations in the flow field. Wells & Stock (1983) proposed expressions for the velocity autocorrelation functions seen by a dense particle, and this approach provides a good comparison with numerical calculations (e.g. Launay, Huilier & Burnage 1999). Pasquill (1974, p. 114) proposed that particle dispersivity

is isotropic when $\mathscr{D}^{(p)} = \mathscr{D}^{(f)}/(1 + v_T/\sqrt{u'^2})$ where $\sqrt{u'^2}$ is a measure of the velocity variance of the flow; Tchen (1947) proposed that $\mathscr{D}^{(p)} = \mathscr{D}^{(f)}/(1+\tau_p/\tau_L)$, where τ_p and τ_L are, respectively, the particle response time and Lagrangian correlation time of the flow. Both expressions suggest that the particle dispersivity decreases monotonically with particle response time. Hunt, Perkins & Fung (1994) analytically studied a one-dimensional model of particles sedimenting through a random flow, and confirmed many of their conclusions numerically. They showed that when particles sediment with a speed comparable to the characteristic translation speed of the vortices, the vertical particle dispersivity $\mathscr{D}_{11}^{(p)}$ was greater than the vertical particle dispersivity $\mathscr{D}_{11}^{(f)}$ and this difference increased with St; for large v_T, the particle dispersivity became much smaller than the fluid dispersivity. The difficulty with calculating dispersivity from velocity autocorrelation functions is that it tends to mask the underlying physics, particularly how straining and vortical regions in a turbulent flow separately influence $\mathscr{D}^{(p)}$. In this paper, both a Lagrangian and velocity autocorrelation method are applied to study particle dispersion.

The motivation for this paper is to explore how the bulk settling speed and dispersivity of particles are influenced by localized coherent vortical structures. Detailed information about particle displacement when it encounters an isolated vortical structure is combined with a statistical description of how the particle encounters the vortex to calculate the bulk settling properties of particles. For this, the methodology of Dávila & Hunt (2001) is developed to account for the effect of boundedness of the flow and the convergence of certain integrals. Work dealing with fluid displacement or drift in potential flows (Darwin 1953), the concept of a partial drift volume (Eames, Belcher & Hunt 1994), and its application to calculating mechanical dispersivity (Eames & Bush 1999) are employed.

The paper is structured as follows: the particle equation of motion and flow field generated by a spherical vortex are described in § 2, along with the definition of the particle drift volume and second moments of displacement. In § 3, an asymptotic analysis of particle displacement and particle sheet deformation is presented for particles with small inertia. These results are applied in § 4 to estimate the bulk settling speed of particles and the longitudinal dispersivity due to a random collection of spherical vortices moving vertical upwards. General conclusions are made in § 5.

2. Mathematical model

The dynamics of small, dense, spherical particles settling in the vicinity of an isolated Hill's spherical vortex steadily translating vertically against gravity will be examined.

2.1. *Particle equation of motion*

Particles moving with velocity $\boldsymbol{v}$ in an unsteady flow $\boldsymbol{u}$ experience a number of forces (Magnaudet & Eames 2000), including a drag force $\boldsymbol{F}_D$, buoyancy force $\boldsymbol{F}_g$, added-mass force $\boldsymbol{F}_A$, inertial force $\boldsymbol{F}_I$, shear induced lift $\boldsymbol{F}_S$ and history force $\boldsymbol{F}_H$. In a number of different cases, it has been demonstrated analytically or numerically (e.g. Magnaudet, Rivero & Fabre 1987; Hunt & Eames 2002) that the total force acting on the body may be reasonably estimated by adding together viscous and inviscid contributions and the force acting on the particle is approximately

$$\frac{\pi}{6} d^3 \rho_p \frac{\mathrm{d}\boldsymbol{v}}{\mathrm{d}t} = \boldsymbol{F}_D + \boldsymbol{F}_g + \boldsymbol{F}_A + \boldsymbol{F}_I + \boldsymbol{F}_S + \boldsymbol{F}_H. \tag{2.1}$$

The drag force is

$$\boldsymbol{F}_D = \tfrac{1}{8}\rho_f \pi d^2 C_D |\boldsymbol{u} - \boldsymbol{v}|(\boldsymbol{u} - \boldsymbol{v}), \tag{2.2}$$

where the drag coefficient $C_D(Re_p)$ is a function of Reynolds number $Re_p = d|\boldsymbol{v}-\boldsymbol{u}|/\nu$ based on the particle slip velocity. When $Re_p \leqslant O(1)$, Stokes drag law (Batchelor 1967)

$$C_D = \frac{24}{Re_p}, \tag{2.3}$$

can be applied.

The net buoyancy force arising from the density contrast between the particle and fluid is

$$\boldsymbol{F}_g = -(\rho_p - \rho_f)\frac{\pi}{6} d^3 g \hat{\boldsymbol{x}}. \tag{2.4}$$

When the particle accelerates, it must also locally accelerate the fluid, and this gives rise to the added-mass force

$$\boldsymbol{F}_A = \rho_f C_m \frac{\pi d^3}{6}\left(\frac{\mathrm{D}\boldsymbol{u}}{\mathrm{D}t} - \frac{\mathrm{d}\boldsymbol{v}}{\mathrm{d}t}\right), \tag{2.5}$$

which is important when the density of the particle is comparable to or less than the density of the ambient fluid. The added-mass coefficient C_m is determined by the particle geometry and takes the value of $1/2$ for spherical particles. The inertial force is

$$\boldsymbol{F}_I = \rho_f \frac{\pi}{6} d^3 \frac{\mathrm{D}\boldsymbol{u}}{\mathrm{D}t}, \tag{2.6}$$

and its origin lies in the force induced by gradients of the ambient pressure field (Magnaudet & Eames 2000). The shear-induced lift force is

$$\boldsymbol{F}_S = \rho_f C_L \frac{\pi}{6} d^3 (\boldsymbol{u} - \boldsymbol{v}) \times \boldsymbol{\omega}, \tag{2.7}$$

and physically arises in high-Reynolds-number flows owing to the stretching of vortical tubes to produce a trailing horse-shoe vortex (Auton 1987), or, in the case of low-Reynolds-number flows (Saffman 1965), asymmetric diffusion of vorticity in the external ambient flow. The history force, $\boldsymbol{F}_H$, is negligible when the response time of the particles is comparable to, or shorter than, the advective timescale of the flow field, and is neglected in this treatment of particle dynamics described here.

By combining the above information, the particle motion is described by the equations:

$$\frac{\mathrm{d}\boldsymbol{x}}{\mathrm{d}t} = \boldsymbol{v}, \tag{2.8}$$

$$\frac{\mathrm{d}\boldsymbol{v}}{\mathrm{d}t} = \frac{\beta}{(\beta + C_m)\tau_p}(\boldsymbol{u} - \boldsymbol{v} - v_T \hat{\boldsymbol{x}}) + \frac{1 + C_m}{\beta + C_m}\frac{\mathrm{D}\boldsymbol{u}}{\mathrm{D}t} + \frac{C_m}{\beta + C_m}\boldsymbol{\omega} \times (\boldsymbol{v} - \boldsymbol{u}), \tag{2.9}$$

where the fall velocity v_T and the particle response time τ_p are related to the relative density of the particle to the fluid (ρ_p/ρ_f) and particle diameter d through

$$v_T = \frac{g(\rho_p/\rho_f - 1)d^2}{18\nu}, \tag{2.10}$$

and

$$\tau_p = \frac{d^2 \rho_p}{\rho_f 18\nu}. \tag{2.11}$$

This formulation is identical to Dávila & Hunt (2001), although they chose to incorporate the density contrast ($(\beta-1)/\beta$) between the fluid and particle into their definition of the response time. The benefit of the above form of the equation of motion, is that it enables 'rigid' fluid particles to be followed when $\beta = 1$.

2.2. *Flow generated by a Hill spherical vortex*

A cylindrical coordinate system (x, y) is employed, with x parallel to gravity and y the distance from the centreline of the vortex. The flow $\boldsymbol{u} = (u_x, u_y)$ is expressed in terms of a Stokes streamfunction Ψ through

$$\boldsymbol{u} = \left(\frac{1}{y}\frac{\partial \Psi}{\partial y}, -\frac{1}{y}\frac{\partial \Psi}{\partial x}\right). \tag{2.12}$$

The streamfunction describing the flow generated by a spherical vortex of radius a, having a centre $h = Ut$, is (Milne-Thomson 1968, p. 578),

$$\Psi(x, y) = \begin{cases} -\dfrac{3U}{4a^2}\left(y^4 + y^2(x-h)^2 - \frac{5}{3}y^2a^2\right) & r < a, \\ \dfrac{Uy^2a^2}{2((x-h)^2+y^2)^{3/2}}, & r > a, \end{cases} \tag{2.13}$$

where $r = \sqrt{(x-h)^2 + y^2}$ is the distance from the vortex centre. Explicit use is made later of the velocity field: within the vortex ($r < a$),

$$u_x = -\frac{3U}{4}\left(4\left(\frac{y}{a}\right)^2 + 2\left(\frac{x-h}{a}\right)^2 - \frac{10}{3}\right), \quad u_y = \frac{3U}{2a^2}y(x-h), \tag{2.14}$$

and outside the vortex ($r > a$)

$$u_x = \frac{Ua^3}{2}\frac{2(x-h)^2 - y^2}{((x-h)^2+y^2)^{5/2}}, \quad u_y = \frac{3Ua^3y(x-h)}{2((x-h)^2+y^2)^{5/2}}. \tag{2.15}$$

The external flow corresponds to a rigid sphere of radius a moving with speed U.

Inside the vortex, the circulation associated with a fluid element, $\Gamma = \omega_\theta/y$, is uniform (as required by the Batchelor–Proudman theorem) so that the azimuthal component of vorticity is proportional to the distance from the centreline,

$$\omega_\theta = \frac{15Uy}{2a^2}. \tag{2.16}$$

Outside the vortex, the flow is irrotational and $\boldsymbol{\omega} = 0$.

The particle equation of motion is rendered dimensionless using the characteristic length and velocity scales corresponding to the vortex radius a and rise speed U: writing $\tilde{\boldsymbol{v}} = \boldsymbol{v}/U$, $\tilde{\boldsymbol{u}} = \boldsymbol{u}/U$, $\tilde{\boldsymbol{x}} = \boldsymbol{x}/a$, $\tilde{t} = Ut/a$, (2.8) and (2.9) reduce to

$$\frac{\mathrm{d}\tilde{\boldsymbol{x}}}{\mathrm{d}\tilde{t}} = \tilde{\boldsymbol{v}}, \tag{2.17}$$

$$\frac{\mathrm{d}\tilde{\boldsymbol{v}}}{\mathrm{d}\tilde{t}} = \frac{\beta}{(\beta + C_m)St}\left(\tilde{\boldsymbol{u}} - \tilde{\boldsymbol{v}} - \frac{v_T}{U}\hat{\boldsymbol{x}}\right) + \frac{1 + C_m}{\beta + C_m}\frac{\mathrm{D}\tilde{\boldsymbol{u}}}{\mathrm{D}\tilde{t}} + \frac{15C_m}{2(\beta + C_m)}\tilde{y}\hat{\boldsymbol{\theta}} \times (\tilde{\boldsymbol{v}} - \tilde{\boldsymbol{u}})\mathrm{H}(1 - \tilde{r}), \tag{2.18}$$

where the Heaviside step function $\mathrm{H}(1-\tilde{r})$ is unity within the vortex and zero outside. The equation contains three dimensionless groups: $St = \tau_p U/a$, $\beta = \rho_p/\rho_f$ and v_T/U. We specifically focus on dense particles, where the limit $\beta \gg 1$ is applied.

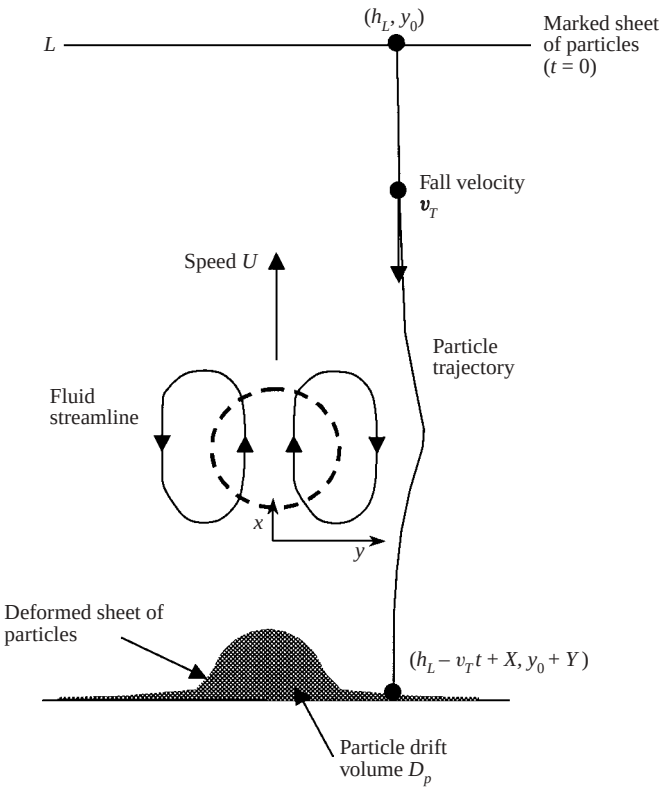

FIGURE 1. Schematic of a sheet of particles sedimenting past a spherical vortex translating vertically upwards.

The analytical results developed in this paper for $St \to 0$, collapse in terms of v_T/U, and for this reason we discuss the solutions in these two variables, rather than the particle Froude number, which forms the basis of the discussion by Dávila & Hunt (2001).

2.3. *Deformed particle sheets and moments of displacement*

Figure 1 shows a schematic of the problem considered. A sheet of particles is released at $t = 0$ a distance h_L far above the vortex. In the absence of the vortex, a particle starting at (h_L, y_0) sediments with speed v_T and its subsequent position is $x = h_L - v_T t$, $y = y_0$. The effect of a translating vortex is to permanently displace the particles both vertically and laterally a distance X and Y, respectively, where

$$X = \int_0^\infty (v_x + v_T)\,\mathrm{d}t = \lim_{t\to\infty}(x - h_L + v_T t), \qquad Y = \lim_{t\to\infty}(y - y_0). \tag{2.19}$$

Since the flow perturbation caused by the vortex is localized, decaying with distance r from the vortex as $\sim Ua^3/r^3$, the permanent displacement (X, Y) is finite everywhere even when $v_T/U = 0$, except on the centreline. This is in contrast to the model of Dávila & Hunt (2001), where the flow field generated by a Rankine vortex decays so slowly with distance that the displacement field is not finite when $v_T/U = 0$.

The particle drift volume (which Dávila & Hunt (2001) refer to as the drift integral) associated with a wide sheet of particles starting infinitely far in front of the vortex

and falling an infinite distance past the vortex is defined here by

$$D_p = \lim_{h_L/y_R \to \infty} \int_0^{y_R} X \, \mathrm{d}A, \tag{2.20}$$

where $\mathrm{d}A = 2\pi y_0 \, \mathrm{d}y_0$. The limit $h_L/y_R \to \infty$ is imposed to ensure that D_p is single valued in unbounded flows. This is a subtle feature of drift volumes which has been discussed by Darwin (1953), Benjamin (1986), and Eames *et al.* (1994). When the flow is bounded by channel walls, there is an additional contribution to the vertical particle displacement which must also be considered and is discussed in § 3.3.

The particle displacement decays sufficiently rapidly with y_0 that the second moments of displacement defined by

$$M_{xx} = \int_0^{\infty} \tfrac{1}{2} X^2 \, \mathrm{d}A, \qquad M_{yy} = \int_0^{\infty} \tfrac{1}{2} Y^2 \, \mathrm{d}A, \tag{2.21}$$

are finite and independent of h_L when the particle sheet starts far in front of the vortex.

For the vertical flow past a random collection of rigid bodies, Eames & Bush (1999) related the longitudinal fluid dispersivity $\mathscr{D}_{11}^{(f)}$ for high-Péclet-number flows to M_{xx}. Dávila & Hunt (2001) showed how the bulk settling speed of dense particles is related to the particle drift volume D_p, but because of the slow decay of the flow perturbation for a Rankine vortex, the methodology described here cannot be applied to study dispersion by a random collection of Rankine vortices. We extend these concepts in § 4 to relate the bulk settling properties of particles through a random collection of vortices to the moments of displacement defined above.

3. Dynamics of small dense particles settling near a spherical vortex

3.1. *Inertialess particles* ($St = 0$)

When $St = 0$, the particles are inertialess and sediment relative to the local flow according to

$$\boldsymbol{v} = \boldsymbol{u} - v_T \hat{\boldsymbol{x}}, \tag{3.1}$$

(e.g. see Maxey 1987). In the frame moving with the vortex the flow is steady and the particle paths can be expressed in terms of a particle streamfunction, Ψ_p:

$$\Psi_p = \begin{cases} -\dfrac{3U}{4a^2}\left(y^4 + y^2(x-h)^2 - \tfrac{5}{3}y^2a^2\right) - \tfrac{1}{2}y^2(U+v_T), & r \leqslant a, \\ \dfrac{Uy^2a^3}{2((x-h)^2+y^2)^{3/2}} - \tfrac{1}{2}y^2(U+v_T), & r > a. \end{cases} \tag{3.2}$$

The particle streamfunction is constant along particle trajectories and far above or below the vortex, tends to the limiting value of

$$\Psi_p \equiv -\tfrac{1}{2}y_0^2(U+v_T), \tag{3.3}$$

where y_0 is the initial distance of the particle from the centreline. According to (3.2) and (3.3) inertialess particles are not permanently displaced laterally (i.e. $Y = 0$). Particles starting far in front of the vortex and greater than a distance $a(v_T/(U+v_T))^{1/2}$ from the centreline do not enter the vortex, while particles entering the vortex encounter a spherical shadow region of radius

$$R = a(1 - 2v_T/3U)^{1/2}, \tag{3.4}$$

from which they are excluded. For $v_T/U > 3/2$, particles sediment through the entire vortex and the shadow region disappears.

The particle drift volume can be calculated by exploiting the geometrical argument of Yih (1985). When the particle sheet starts infinitely far infront of the vortex and the vortex translates an infinite distance, the drift volume is

$$D_p = \frac{4\pi\mu}{v_T + U} - V_S. \tag{3.5}$$

From (3.2), the volume of the shadow region is $V_S = 4\pi R^3/3$ and the strength of the dipole moment characterizing the particle streamlines far from the vortex is $\mu = (1 + C_m)UV/4\pi$ (where $C_m = 1/2$). Substituting these expressions into (3.5) yields

$$D_p = \frac{2\pi a^3}{v_T/U + 1} - \frac{4\pi a^3}{3}\left(1 - \frac{2}{3}\frac{v_T}{U}\right)^{3/2} \tag{3.6}$$

for $v_T/U < 3/2$, and

$$D_p = \frac{2\pi a^3}{v_T/U + 1} \tag{3.7}$$

for $v_T/U \geqslant 3/2$. As v_T/U increases from zero, D_p initially increases because the volume of the shadow region (second term on the right-hand side of (3.6)) decreases faster than the dipole moment (first term on the right-hand side of (3.6)) which characterizes the far-field flow. For large values of v_T/U, the vertical particle displacement decreases because particles spend less time near the vortex; thus the particle drift volume has a maximum value at $v_T/U = 1.398$ of $0.810\pi a^3$, which is larger than Darwin's drift volume ($2\pi a^3/3$).

Close to the centreline ($y_0/a \ll 1$), the vertical displacement is controlled by the particle streamline curvature near the particle stagnation points (PSPs), so it can be shown (Eames *et al.* 1994) that

$$X(y_0) \approx \frac{4a(1 - 2v_T/3U)^{1/2}}{3} \log\left(\frac{2a(1 - 2v_T/3U)^{1/2}3^{3/4}}{y_0}\right). \tag{3.8}$$

From (3.2), the particle streamlines far from the centreline ($y_0/a \gg 1$) are equivalent to the streamlines past a sphere of radius R, so the vertical particle displacement is (Eames *et al.* 1994)

$$X(y_0) \approx \frac{9\pi a^6}{64(v_T/U + 1)^2 y_0^5}. \tag{3.9}$$

When $v_T/U \gg 1$, the particles sediment with an approximately straight trajectory. In this limit, the vertical displacement is

$$\begin{aligned} X(y_0) &= \int_0^\infty (v_x(X + h_L - (v_T + U)t, y) + v_T)\,\mathrm{d}t \\ &\approx \int_0^\infty u_x(h_L - (v_T + U)t, y_0)\,\mathrm{d}t \\ &= \frac{5a}{v_T/U + 1}\left(1 - \frac{y_0^2}{a^2}\right)^{3/2}. \end{aligned} \tag{3.10}$$

Particles which do not pass through the vortex ($y_0/a > 1$) suffer a negligible permanent vertical displacement because they experience equal positive and negative flow perturbations which cancel each other out. When $y_0/a \leqslant 1$, the vertical symmetry

of the flow perturbation is broken and the particles experience a slightly higher vertical flow inside the vortex and thus are displaced vertically upwards as described by (3.10). The corresponding second moments of displacement are

$$M_{xx} = \frac{25\pi a^4}{8(v_T/U+1)^2}, \qquad M_{yy} = 0. \tag{3.11}$$

Equation (3.7) can also be recovered from (3.10). For inertialess, neutrally buoyant particles ($v_T = 0$), $D_p = 2\pi a^3/3$, $M_{xx} = 0.38a^4$ and $M_{yy} = 0$ (Eames & Bush 1999).

3.2. *Weakly inertial particles* ($St \ll 1$)

When $St \ll 1$, the particle velocity

$$\boldsymbol{v} \sim \boldsymbol{u} - v_T\hat{\boldsymbol{x}} + \tau_p\left(\frac{\partial \boldsymbol{u}}{\partial t} + \boldsymbol{u}\cdot\nabla\boldsymbol{u} - v_T\frac{\partial \boldsymbol{u}}{\partial x}\right) \tag{3.12}$$

(see the derivation by Maxey 1987). The divergence of the particle velocity field is then

$$\nabla\cdot\boldsymbol{v} = \tau_p\left(\nabla^2\left(\tfrac{1}{2}u^2\right) - \nabla\cdot(\boldsymbol{u}\times\boldsymbol{\omega})\right). \tag{3.13}$$

The consequence of inertia is therefore to cause the particle trajectories to diverge or converge (and therefore cross) and (3.13) shows that crossing trajectories are intimately related to the presence of vorticity. The region corresponding to $\nabla\cdot\boldsymbol{v} < 0$, is

$$|x-h| < \sqrt{4/3}|y|, \qquad (x-h)^2 + y^2 < a^2, \tag{3.14}$$

while outside this region and the vortex, $\nabla\cdot\boldsymbol{v} > 0$. The effect of inertia leads to a permanent lateral displacement which in the limit of $v_T/U \gg 1$ is approximately

$$Y(y_0) \approx -\frac{\tau_p}{v_T+U}\int_{-\infty}^{\infty}\left(u_x\frac{\partial}{\partial x} + u_y\frac{\partial}{\partial y}\right)u_y\,\mathrm{d}x. \tag{3.15}$$

Substituting (2.14) and (2.15) into the above equation yields

$$Y(y_0) \approx \begin{cases} \dfrac{2aSt}{1+v_T/U}\displaystyle\int_0^{\sin^{-1}(y_0/a)}\left(\frac{15}{4}\sin^6\theta - 3\sin^8\theta\right)\mathrm{d}\theta, & \\ -\dfrac{2aSt}{1+v_T/U}\left(1-\dfrac{y_0^2}{a^2}\right)^{1/2}\dfrac{y_0}{a}\left(\dfrac{15}{4}-\dfrac{9}{2}\dfrac{y_0^2}{a^2}\right) & y_0 \leqslant a. \\ \dfrac{15\pi a^7 St}{32(1+v_T/U)y_0^6} & y_0 > a. \end{cases} \tag{3.16}$$

The lateral displacement scales as $\sim aSt/(1+v_T/U)$ and is extremely localized, decaying rapidly from the centreline as $\sim a^7 St/y_0^6(1+v_T/U)$. Particles passing close to or far from the centreline, spend most of their time in a region where $\nabla\cdot\boldsymbol{v} \gtrless 0$ so that $Y \gtrless 0$.

The weighted moment of lateral displacement, calculated numerically by substituting (3.16) into (2.21), is

$$M_{yy} \sim \frac{1.21\pi a^4 St^2}{(v_T/U+1)^2}. \tag{3.17}$$

Thus the weighted moment M_{yy} is sensitive to the particle Stokes number, even for large settling velocities, while the influence of weak inertia on M_{xx} is negligible.

3.3. *Reflux contributions: the effect of bounding walls*

In an unbounded flow, the integral of vertical displacement across the entire flow, $\int_{A_\infty} X \, \mathrm{d}A$, is non-convergent, and for this reason the limiting constraint that the particle sheet starts infinitely far infront of the vortex is applied in the evaluation of the particle drift volume (see (2.20)). This is a well-known feature of drift volumes, being related to the slow decay of the velocity perturbation in unbounded flows, and has been discussed previously by Benjamin (1986) and Eames *et al.* (1994). In a bounded flow (of cross-sectional area A), these problems are not encountered because a return flow or reflux is necessarily introduced by the sidewalls. To understand the influence of bounding walls on D_p, we first discuss the main results for the distortion of a sheet of *fluid particles* in a channel flow. In a bounded channel flow, a body of volume V, whose shape is characterized by an added-mass coefficient C_m, displaces a volume $C_m V$ forward owing to the increased residence time of fluid particles which pass near the body. By mass conservation, there is a return flow or reflux volume $(C_m + 1)V$ corresponding to the sum of the drift volume and the volume of the body. The return flow leads to a weak reflux or negative displacement, X_r, which is spread uniformly across the channel, and is equal to

$$X_r = \int_{-\infty}^{\infty} \frac{u_x(x, y)}{U} \, \mathrm{d}x = \frac{[\phi]_{x=-\infty}^{\infty}}{U} = -\frac{V(C_m + 1)}{A}. \tag{3.18}$$

For bounded flows, we must also consider the influence of a return flow or reflux on particle displacement. A translating vortex also generates a weak return flow which tends to increase the fall speed of particles far from the vortex. The advective timescale based on the return flow scales as $A^{1/2}/U$ and depends on the cross-sectional area of the channel A. Since the pressure field decreases rapidly from the vortex (as $\sim \rho_f U^2 a^6 / r^6$) and the exterior flow is irrotational, both the buoyancy force (arising from gradients in pressure) and the lift force, are negligible or zero. Thus the inertialess approximation (described by (3.1)) is applicable in the far field because the container size can be made large enough that the Stokes number $\tau_p U / A^{1/2} = aSt/A^{1/2}$ based on the advective timescale associated with the return flow, is small. In this limit, the reflux particle displacement is

$$\begin{aligned} X_r &= \int_{-\infty}^{\infty} \frac{u_x(X + h_L - (v_T + U)t, y)}{U} \, \mathrm{d}t \\ &\approx \int_{-\infty}^{\infty} \frac{u_x(\tau, y)}{v_T + U} \, \mathrm{d}\tau = -\frac{V(C_m + 1)}{A(v_T/U + 1)}, \end{aligned} \tag{3.19}$$

independent of St. Although the far-field displacement (3.19) is small, its integral across the channel,

$$\int_A X_r \, \mathrm{d}A = -\frac{V(C_m + 1)}{(v_T/U + 1)} = -\frac{2\pi a^3}{(v_T/U + 1)}, \tag{3.20}$$

is comparable to the particle drift volume. Thus for a vortex translating vertically in a wide channel, the sum of the particle drift volume and reflux volume is

$$D_p - \frac{2\pi a^3}{(v_T/U + 1)}. \tag{3.21}$$

For inertialess particles ($St = 0$), the volume displaced forward in a bounded channel is $-V_S$ which corresponds to the volume of the shadow region.

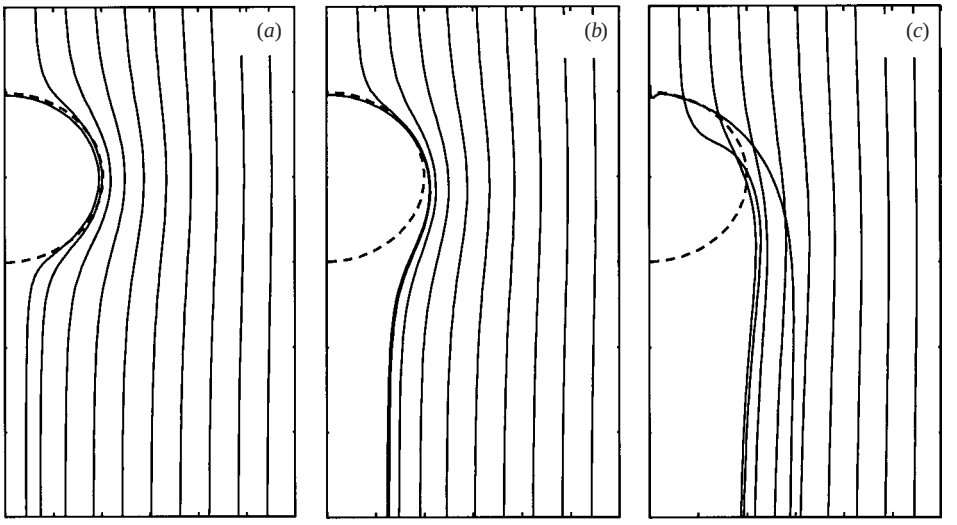

FIGURE 2. Trajectories of dense particles in the frame moving with the vortex are shown for fixed $v_T/U = 0.1$ and for (*a*) $St = 0.01$, (*b*) $St = 0.1$ and (*c*) $St = 1.0$. The edge of the vortex is shown by the dashed curve. Note the crossing trajectories in (*c*).

The global kinematic constraints on the flow in terms of any bounding horizontal walls or the manner in which the vortices are introduced into the flow have a subtle but important effect on particle displacement. A vortex may be generated either by the local application of a force to the fluid or by a volumetric injection of fluid (such as from a piston). In the latter case, a volumetric source is introduced into the flow and its contribution to the particle displacement must also be considered. In the former case, which we consider, no source is introduced.

3.4. *Numerical results for finite St*

The influence of finite St and v_T/U on the trajectories of particles around and through a translating vortex was explored numerically by integrating the equation of motion (2.18). Particles were released far above the vortex, from (h_L, y_0), with an initial velocity $\boldsymbol{v}(0) = -v_T\hat{\boldsymbol{x}} + \boldsymbol{u}(h_L, y_0)$. Providing $h_L/a \gg 1$, the numerical results correspond to the particles being released infinitely far above the vortex. In all the calculations, the ratio of particle to fluid density, β, was fixed at 1000.

Figure 2 shows the trajectories of dense particles sedimenting in the frame moving with the vortex and illustrates the significant influence of the particle Stokes number. For low particle inertia, $St \ll 1$, the shadow region where the particles are excluded is roughly spherical. As St increases, the asymmetry of the shadow region increases. Figure 2(*c*) illustrates the crossing of particle trajectories, which is associated with the inertia of the particles. Note that when $St = 1$, the actual particle trajectories will be influenced by history forces, and the figure illustrates the effects of increasing particle inertia.

Figure 3 shows the trajectories of particles released close to the centreline ($y_0/a = 0.001$) for increasing values of v_T/U and for three different values of St. These figures show the geometry of the shadow region inside the vortex and the downstream shadow tail. For $St = 0.01$, the shadow region is approximately spherical and centred on the vortex and is virtually contained within it. As v_T/U increases, the radius of the shadow region decreases until it disappears at $v_T/U = 3/2$. As St increases, the

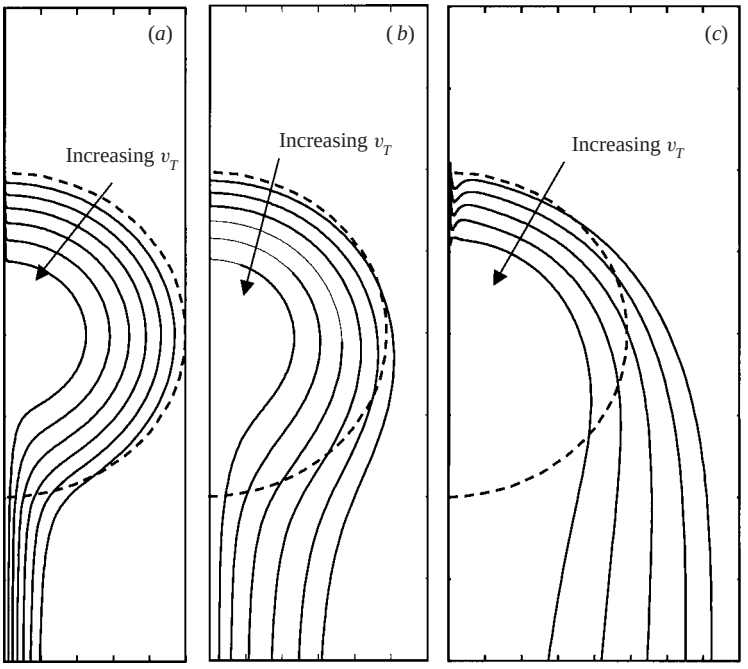

FIGURE 3. Trajectories of dense particles released close to the centreline ($y_0/a = 0.001$) are shown in the frame of reference moving with the vortex for (*a*) $St = 0.01$, (*b*) $St = 0.1$ and (*c*) $St = 1.0$. The different trajectories show the effect of increasing $v_T/U = 0.2$, 0.4, 0.6, 0.8, 1.0, 1.2 and 1.4. The dashed curve corresponds to the edge of the vortex.

asymmetry of the trajectories increases with a growing tail region below the spherical head. Eventually the spherical part of the shadow region can no longer be clearly identified. For $St = 1$, particles overshoot the particle stagnation point at the front of the vortex, which leads to particles spending an increased time near the vortex.

The shadow region was characterized in terms of r_m the minimum distance of a particle streamline from the centre of the vortex, generated by a particle released close to the centreline. The width of the downstream shadow region, $2w$, corresponds to the final lateral position of the particle far below the vortex, as shown in figure 4. Figures 4(*a*) and 4(*b*) show how r_m and w vary with particle fall speed (v_T/U). As St decreases, the radius of the shadow region tends to the theoretical prediction of (3.4) and the asymmetry of the particle separation streamline (as measured by w/a) is reduced.

The permanent particle displacement formed by sheets of particles sedimenting past the translating vortex are shown in figure 5. The displacement is plotted as a function of the initial lateral position of the particle. Figure 5(*a*) shows the vertical permanent particle displacement for $St = 0.1$ and increasing values of v_T/U. When $v_T/U = 3$, there are no PSPs and particles sediment through the vortex so that there is no singularity in the vertical displacement. For $v_T/U < 3/2$, it is shown in figure 4(*b*) that $r_m > 0$ and therefore a PSP exists. Particles passing near a PSP spend a long time there and as with fluid particle displacement near stagnation points, the particle displacement suffers a logarithmic singularity. When $St = 1$ (see figure 5*b*), the particles spend an increased time near the vortex because they overshoot the PSP, and the particle displacement (which is a measure of the particle residence time near

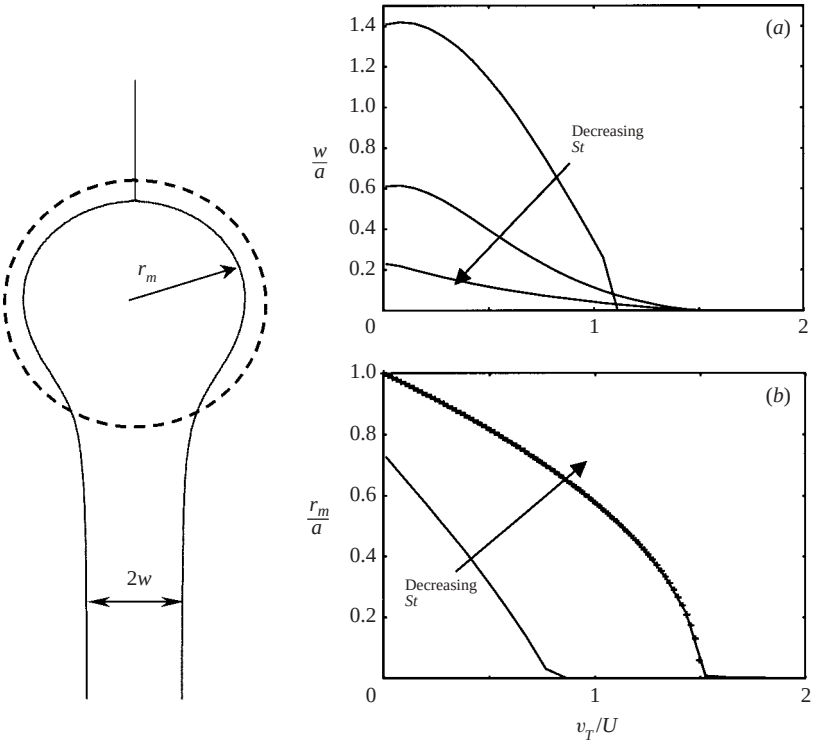

FIGURE 4. Schematic showing the shadow region generated by a particle sedimenting relative to the vortex frame of reference. The characteristic shape is defined in terms of the final width $2w$ of the tail of the shadow region, and the minimum distance from the vortex centre, r_m. In (a) and (b), w and r_m are plotted as functions of v_T/U for $St = 0.01$, 0.1 and 1.0. In (b), the minimum radius r_m based on the inertialess particle approximation (3.4), $St = 0$, is plotted with $+$. The lines for both $St = 0.1$ and $St = 0.01$ are coincident with each other and the inertialess approximation.

the vortex) is significantly increased (compare the scales of figures 5a and 5b). In addition, the permanent vertical displacement does not decrease monotonically with distance from the centreline because of the circulation of particles within the vortex at intermediate distances. Figure 5(c) shows a comparison between the displacement field, suitably rescaled, and the prediction (3.10) with good agreement for high values of v_T/U. The lateral displacement of the particles for $St = 0.1$ is shown in figure 5(d). It can be seen that for high values of v_T/U it is possible for some particles to have a negative displacement, but for low values it is always positive.

The effect of particle inertia on their divergence and lateral displacement is shown in figure 6. The regions of the flow corresponding to $\nabla \cdot \boldsymbol{v} > 0$, < 0, and 0, are shown in figure 6(a). Close to the centreline (in the white region) particle trajectories tend to move inwards with a minimum at a distance $a/\sqrt{7}$ from the centreline. A comparison between the analytical result and numerical computations for lateral displacement for $St = 0.001$ and $v_T/U = 10$ is shown in figure 6(b), and the agreement is good.

Numerical calculations for the moments of displacement (D_p, M_{xx} and M_{yy}) are shown in figure 7. For particles with small inertia, figure 7(a) shows the particle drift volume, D_p initially increases with v_T/U until it reaches a maximum when $v_T/U \sim 1$, beyond which it decreases rapidly. This general trend follows that predicted by (3.6)

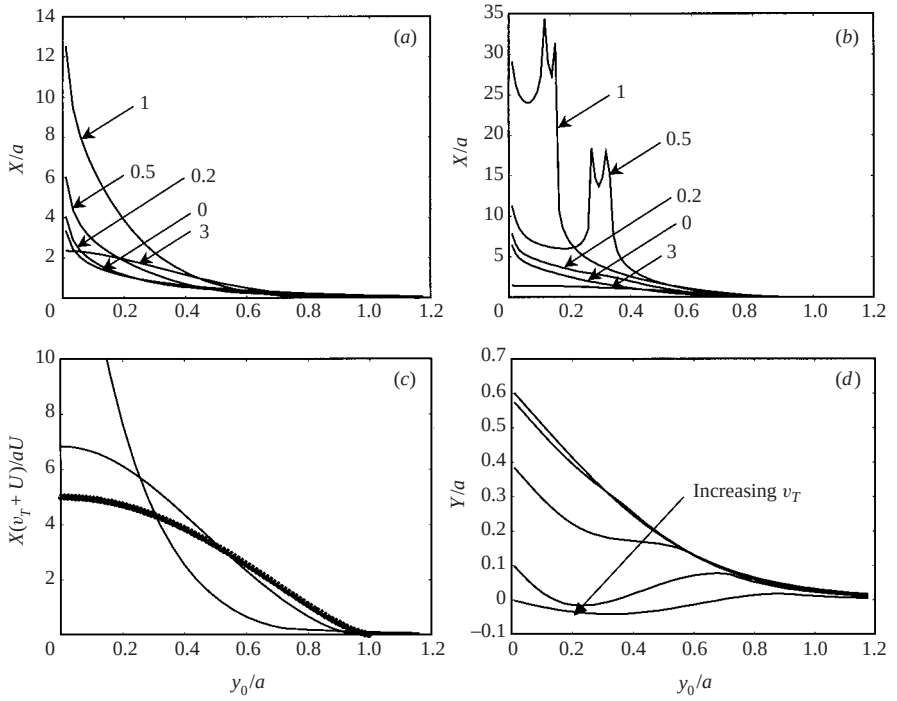

FIGURE 5. Vertical displacement of particles, X, sedimenting through the vortex, as a function of their initial lateral position, y_0. (a) and (b) show the contrasting effect of increasing the Stokes number from $St = 0.1$ (in (a)), to $St = 1$ (in (b)), for $v_T/U = 0$, 0.2, 0.5, 1 and 3. (c) shows a comparison with the rescaled X with $aU/(v_T + U)$, and the analytical prediction (3.6) which is based on the approximation $St \ll 1$ and $v_T/U \gg 1$. The lateral displacement, Y, is shown in (d), $St = 0.1$ and $v_T/U = 0.0$, 0.2, 0.5, 1.0 and 3.0.

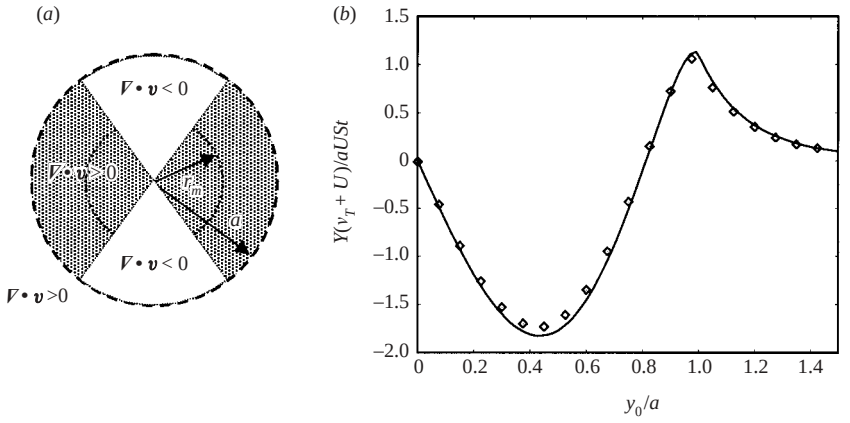

FIGURE 6. (a) Schematic of the regions where $\nabla \cdot \boldsymbol{v}$ is negative, positive or zero. (b) Comparison between an asymptotic expression for lateral displacement (3.16) in the limits of $St \ll 1$ and $v_T/U \gg 1$ with numerical calculations for $St = 0.001$ and $v_T/U = 10$.

and (3.7), which is based on the inertialess particle approximation. When $v_T/U > 3/2$, D_p is insensitive to St, but when $v_T/U > 3/2$, though the trend is consistent, the maximum value of D_p increases markedly with St. Figure 7(b)shows the variation of

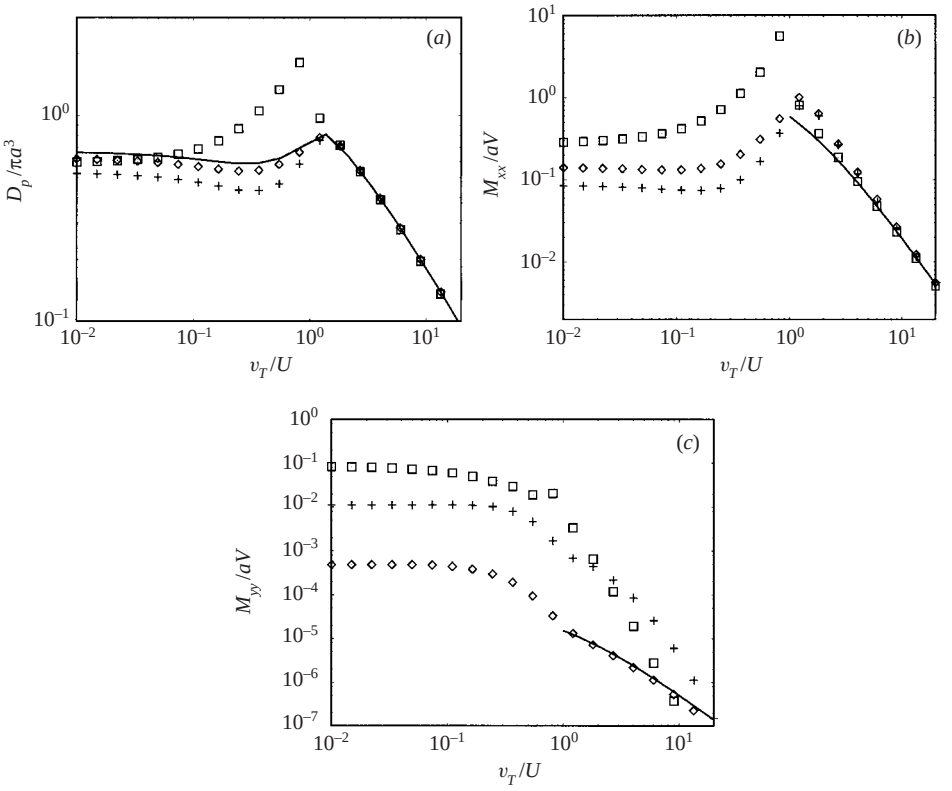

FIGURE 7. Variation of (*a*) particle drift volume, D_p, and (*b*) and (*c*) second moments of displacement, M_{xx} and M_{yy}, as functions of v_T/U for $St = 0.01(\diamond)$, $0.1(+)$ and $1.0(\square)$. The lines represent the analytical results (3.6), (3.7) in (*a*), (3.11) in (*b*), and (3.17) in (*c*).

M_{xx} with v_T/U and agrees very well with (3.11) when it can be applied, $v_T/U > 3/2$. As for D_p, the maximum value of M_{xx} increases with St, as would be expected because as St increases the particles overshoot the PSP, which significantly increases their residence time in this region, leading to a larger vertical displacement. The influence of particle inertia is to lead to particles being displaced laterally so that M_{yy} is sensitive to St and decreases monotonically with v_T/U, as shown in figure 7(*c*). For small St, numerical calculations of M_{yy} agree with (3.17).

4. Mean properties of particles settling through a random distribution of spherical vortices

The bulk properties of particles sedimenting through a random collection of vortices can be calculated by applying the results for the distortion of a particle sheet by one vortex. The velocity decays rapidly with distance from the vortex, so that for a dilute array of such vortices the hydrodynamic interaction between them is weak. As argued by Eames & Bush (1999), the permanent distortion of a particle sheet consists of a localized drift and a non-local reflux contribution, and when the volume fraction of vortices $\alpha \ll 1$, these two effects can be superimposed to estimate the total particle displacement.

4.1. *Bulk settling velocity*

The bulk settling velocity is calculated in terms of the average distance particles move in a time t:

$$\langle v_T \rangle_B = \lim_{t\to\infty} \frac{h_L - \langle x(t) \rangle}{t}, \tag{4.1}$$

where $\langle x(t) \rangle$ is the vertical position of the particles averaged across the whole flow. This definition is equivalent to the particle Lagrangian mean defined by Dávila & Hunt (2001) and corresponds to the approach adopted by Eames & Bush (1999).

The average distance moved by the particles is related to their average vertical displacement through

$$h_L - \langle x(t) \rangle = v_T t - \langle X \rangle, \tag{4.2}$$

where $\langle X \rangle$ is the average displacement and therefore must be the sum of the average displacements owing to drift and reflux. Therefore, from (3.21),

$$\langle X \rangle = \frac{1}{A} \int_A X \, \mathrm{d}A = \frac{N}{A} \left(D_p - \frac{2\pi a^3 U}{v_T + U} \right). \tag{4.3}$$

The number of vortices that have passed through the particle sheet in time t is $N = A(U + v_T)t\alpha/V$, so the bulk fall velocity is

$$\langle v_T \rangle_B = v_T - \frac{\alpha(U + v_T)}{V} \left(D_p - \frac{2\pi a^3}{v_T/U + 1} \right). \tag{4.4}$$

This result, as with Dávila & Hunt (2001), does not depend on the vortices being randomly positioned.

For inertialess particles ($St = 0$), the bulk fall speed is

$$\langle v_T \rangle_B = v_T + \frac{\alpha(U + v_T)V_S}{V}. \tag{4.5}$$

Thus the increase in the fall velocity is related geometrically to the volume fraction of shadow regions in the flow. This is an entirely general result for flows that are steady in the frame moving with the vortex or for 'frozen' turbulence.

Dávila & Hunt (2001) noted that the definition of the mean fall speed of Maxey (1987), based on randomly placing particles everywhere in the flow, leads to the conclusion that the average fall speed for inertialess particles is equal to v_T; however, this is only because it includes contributions from particles placed in shadow regions, which, according to our calculations, they are not able to enter from the outside. When $v_T/U > 3/2$, the particles fall throughout the vortices and sample the entire flow, so their bulk fall velocity is unchanged from v_T.

Figure 8 shows the fractional increase in the bulk settling velocity as a function of v_T/U and for different values of St. The regions where $\langle v_T \rangle_B - v_T$ is negative correspond to where there is a decreased fall velocity owing to the increased residence time caused by particles overshooting the PSP. The regions where $\langle v_T \rangle_B - v_T$ is positive correspond to where there is an increased fall velocity owing to the return flow induced by the rising shadow region. These two physical processes are identical to those discussed by Dávila & Hunt (2001). In the limit of $v_T/U \to 0$, the average fall speed tends to a non-zero value, $\langle v_T \rangle_B = \alpha U$, corresponding to the volume of the shadow region. These calculations underline that average settling properties are sensitive to how the vortices (or turbulence) are generated (see above, § 3.3).

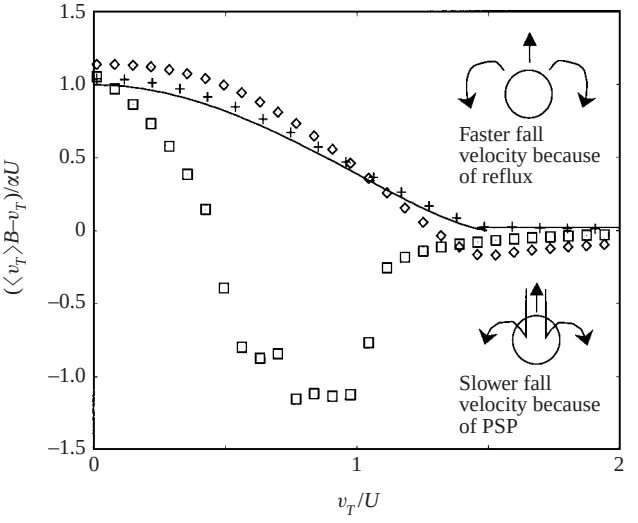

FIGURE 8. Change in the bulk settling velocity of the particles through a random array of steadily rising vortices as a function of the terminal fall speed for $St = 0.01(\diamond)$; $0.1(+)$ and $1.0(\square)$. The line represents the analytical result (4.4).

4.2. *Particle dispersivity*

The dispersion of fluid particles by translating bodies in a bounded potential flow was examined by Eames & Bush (1999) who related vertical fluid dispersivity $\mathscr{D}_{11}^{(f)}$ to M_{xx}. In the following problem, the lateral displacement of fluid particles that encounter a vortex is zero, therefore the lateral fluid-particle dispersivity is zero, i.e. $\mathscr{D}_{22}^{(f)} = \mathscr{D}_{33}^{(f)} = 0$.

The particle dispersivity arising from particles interacting with randomly positioned vortices can be calculated by extending the methodology of Eames & Bush (1999) and randomly superimposing the Lagrangian particle permanent displacements because of encounters with individual vortices. This yields

$$\mathscr{D}_{11}^{(p)} = \lim_{t\to\infty} \frac{\langle (X - \langle X\rangle)^2\rangle}{2t} = \frac{M_{xx}}{V}\alpha(U + v_T). \tag{4.6}$$

Since the flow generated by an individual vortex is symmetric about the stagnation streamline and the mean lateral displacement caused by an isolated vortex is zero. The lateral dispersivity is then

$$\mathscr{D}_{22}^{(p)} = \mathscr{D}_{33}^{(p)} = \lim_{t\to\infty} \frac{\frac{1}{2}\langle Y^2\rangle}{2t} = \frac{M_{yy}}{2V}\alpha(U + v_T). \tag{4.7}$$

The factor of $1/2$ arises because the coordinate axis y is the radial distance from the centreline of a vortex.

Figure 7(b) shows the variation of M_{xx} with particle fall velocity; the corresponding variation of $\mathscr{D}_{11}^{(p)}$ is similarly behaved and differs only by a multiplicative factor $\alpha(U + v_T)$ from M_{xx}/V. Comparison with the results for fluid particles, where $M_{xx} = 0.36a^4$, shows that for finite values of St, dense particles are dispersed vertically at a much faster rate than fluid particles (for $v_T/U \sim 1$) owing to the particles overshooting the PSP and spending an increased time in the vicinity of the vortex. As the particle

fall velocity is increased, the particle dispersivity decreases rapidly, as

$$\mathscr{D}_{11}^{(p)} = \frac{75\alpha U a}{32(v_T/U+1)}, \tag{4.8}$$

and is much smaller than that for fluid particles. The conclusion from these calculations is that the longitudinal particle dispersivity does not decrease monotonically with fall speed, and that it decreases with the inverse of the particle fall speed for $v_T/U \gg 1$. The trend of $\mathscr{D}_{11}^{(p)}$ with v_T is identical to that calculated by Fung *et al.* (2003), with a maximum when v_T is comparable to the translation speed of the vortex, and which ultimately decreases as $\sim 1/(v_T/U+1)$.

Figure 7(*c*) shows the variation of M_{yy} with fall speed; again the corresponding variation of $\mathscr{D}_{22}^{(p)}$ and $\mathscr{D}_{33}^{(p)}$ behave similarly and differ only by a multiplicative factor $\alpha(U+v_T)/2$ from M_{yy}/V. Fluid particles are not dispersed laterally when they encounter an isolated vortex, and thus the lateral dispersivity of fluid particles, $\mathscr{D}_1^{(f)}$, is zero. The numerical calculations show that dispersion perpendicular to the direction of gravity is only significant for $v_T/U < 1$, but this increases further with particle Stokes number. As demonstrated in § 3.4, lateral dispersion arises from the inertia of the particles. For weakly inertial particles sedimenting with a large fall velocity, the lateral dispersivity is

$$\mathscr{D}_{22}^{(p)} = \mathscr{D}_{33}^{(p)} = \frac{0.812\alpha a U St^2}{v_T/U+1}, \tag{4.9}$$

and is thus sensitive to the particle Stokes number.

An alternative, but equivalent, view of understanding how particles are dispersed by a random collection of vortices can be obtained by calculating the Lagrangian autocorrelation of the particle velocity field. Equivalent definitions of the vertical and lateral dispersivities to (4.6) and (4.7) are

$$\mathscr{D}_{11}^{(p)} = \lim_{t\to\infty}\left\langle X\frac{\mathrm{d}X}{\mathrm{d}t}\right\rangle, \qquad \mathscr{D}_{22}^{(p)} = \mathscr{D}_{33}^{(p)} = \frac{1}{2}\lim_{t\to\infty}\left\langle Y\frac{\mathrm{d}Y}{\mathrm{d}t}\right\rangle. \tag{4.10}$$

The particle dispersivities can be re-expressed in terms of the Lagrangian autocorrelation functions (R_{11}, R_{22})

$$\mathscr{D}_{11}^{(p)} = \int_0^\infty R_{11}(\tau)\,\mathrm{d}\tau, \quad \mathscr{D}_{22}^{(p)} = \int_0^\infty R_{22}(\tau)\,\mathrm{d}\tau, \tag{4.11}$$

where

$$\left.\begin{aligned} R_{11}(\tau) &= \langle (v_x(t)+v_T)(v_x(t-\tau)+v_T)\rangle \\ &= \frac{\alpha(U+v_T)}{V}\int_{-\infty}^{\infty}(v_x(t)+v_T)(v_x(t-\tau)+v_T)\,\mathrm{d}t\,\mathrm{d}A, \\ R_{22}(\tau) &= \frac{1}{2}\langle v_y(t)v_y(t-\tau)\rangle \\ &= \frac{\alpha(U+v_T)}{2V}\int_{-\infty}^{\infty}v_y(t)v_y(t-\tau)\,\mathrm{d}t\,\mathrm{d}A. \end{aligned}\right\} \tag{4.12}$$

For inertialess particles ($St \ll 1$) sedimenting rapidly through the fluid, the Lagrangian autocorrelation functions are proportional to the velocity fluctuations

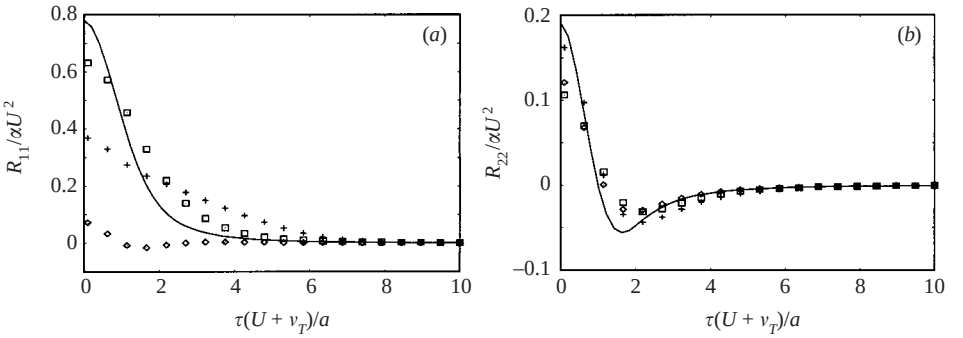

FIGURE 9. The Lagrangian autocorrelation functions R_{11} and R_{22} are plotted in (a) and (b), respectively. The full curves denote (4.13) and (4.14), respectively. The calculations correspond to fixed $St = 0.1$ and v_T/U=0.1 ($\diamond$), 1.0 (+), 5.0 ($\square$).

integrated over the whole flow domain (V_∞) through

$$R_{11}(\tau) = \frac{\alpha}{V}\int_{V_\infty} u_x(x, y)u_x(x - \tau(v_T + U), y)\,\mathrm{d}V_\infty, \tag{4.13}$$

$$R_{22}(\tau) = \frac{\alpha}{2V}\int_{V_\infty} u_y(x, y)u_y(x - \tau(v_T + U), y)\,\mathrm{d}V_\infty, \tag{4.14}$$

because the vertical slip velocity of the particles is equal to their fall speed.

Figure 9 shows numerical calculations of the Lagrangian autocorrelation functions as functions of the lag time τ. Since the trajectories of the particles are determined by their initial lateral position (y_0) and the fluid velocity is steady in the frame moving with the vortex, the autocorrelation of the velocity may be calculated by tracking two material sheets, initially separated by a distance $\tau(U + v_T)$. The full lines correspond to the inertialess particle approximation described by (4.13) and (4.14). Figure 9(a) shows the variation of the vertical velocity correlation (R_{11}) as a function of τ. For $v_T/U \ll 1$, R_{11} decreases rapidly with τ and has a negative minima corresponding to $\tau \sim U/a$. This is associated with the fact that for $\tau \sim U/a$, R_{11} is dominated by contributions from particles experiencing both positive fluid velocity near the front of the vortex and negative velocity at the sides of the vortex – the advective time scale between these two regions is a/U. For $v_T/U > 3/2$, R_{11} is dominated by contributions from particles passing through the vortex where the fluid velocity is positive and R_{11} is positive for all τ.

Figure 9(b) shows the variation of the lateral autocorrelation function (R_{22}) as a function of τ. The negative loop at $\tau \sim a/(U + v_T)$ is associated with the fact that particles are pushed away from the centreline above the vortex, and drawn towards the centreline below the vortex. The integral under the R_{22} curve is identically zero for inertialess particles because they are not dispersed laterally. Figure 9 shows that the characteristic timescale over which particle velocities remain correlated scales with $a/(v_T + U)$. The influence of particle inertia (St) is to increase the particle slip velocity by $\sim StU$, and while the time scale over which the velocities remain correlated, which scales as $a/(v_T + U)$, increases with St, this is of secondary importance. From these observations, the characteristic scales of $\mathscr{D}_{11}^{(p)}$ and $\mathscr{D}_{22}^{(p)}$ can be recovered. While the Lagrangian autocorrelation method of calculating $\mathscr{D}^{(p)}$ is identical to the particle sheet method introduced, it is based on rather detailed calculations of the average velocity autocorrelation functions which tend to mask the underlying physics.

5. Concluding remarks

A detailed theoretical study of the permanent displacement of particles interacting with a localized, steadily translating spherical vortex has been presented. To understand and quantify the bulk settling properties of particles sedimenting through a random collection of vortices, we have applied the idea of drift and developed the concept of the particle drift volume and weighted moments of displacement. This methodology provides a useful framework to quantify the bulk settling properties, in particular the particle dispersivity. This approach provides a means of physically interpreting how particles are dispersed because it is based on a detailed Lagrangian calculation of displacement, and this can be reconciled with the less physically clear approach that employs the Lagrangian velocity autocorrelation function. We have been able to demonstrate that particles may be dispersed faster than fluid particles because inertia increases particle residence time near PSPs. For large fall velocities, particles are dispersed more slowly than fluid particles and the longitudinal dispersivity is inversely proportional to their terminal fall speed. The lateral dispersivity is sensitive to particle Stokes number. Although the calculations are built around a particular flow where vortices are propagating in one direction, the underlying scalings developed for large v_T/U will be preserved for other flows dominated by coherent structures.

As with the concept of the drift volume for inviscid flows, the far field influence of boundaries and the non-absolutely convergent nature of certain integrals needs to be carefully considered. We have resolved the issue of the influence of bounding vertical walls and shown that a weak reflux flow is generated by a translating vortex, whose integrated effect has a significant influence on the bulk settling velocity of the particles. When the flow is bounded by a horizontal surface, these new results indicate that the mechanism by which the vortices or turbulence are generated must also be considered because a vortex may be generated either by an input of momentum or the injection of a finite volume of fluid. This highlights the subtle influence of the global mass constraints and boundaries on the bulk settling properties of dense particles.

I. E. gratefully acknowledges support through an EPSRC Advanced Research Fellowship held at University College London.

REFERENCES

Auton, T. 1987 The lift force on a spherical body in a rotational flow. *J. Fluid Mech.* **183**, 199–218.

Batchelor, G. 1967 *An Introduction to Fluid Dynamics*. Cambridge University Press.

Batchelor, G. & Nitsche, J. 1994 The expulsion of particles from a buoyant blob in a fluidized bed. *J. Fluid Mech.* **278**, 63–81.

Benjamin, T. 1986 Note on added mass and drift. *J. Fluid Mech.* **169**, 251–256.

Csanady, G. 1963 Turbulent diffusion of heavy particles in the atmosphere. *J. Atmos. Sci.* **20**, 201–208.

Darwin, C. 1953 A note on hydrodynamics. *Proc. Camb. Soc. Phil.* **49**, 342–352.

Dávila, J. & Hunt, J. 2001 Settling of small particles near vortices and in turbulence. *J. Fluid Mech.* **440**, 117–145.

Eames, I., Belcher, S. & Hunt, J. 1994 Drift, partial drift and Darwin's proposition. *J. Fluid Mech.* **275**, 201–223.

Eames, I. & Bush, J. 1999 Longitudinal dispersion by bodies fixed in a potential flow. *Proc. R. Soc. Lond.* A **455**, 3665–3686.

Fung, J., Hunt, J. & Perkins, R. 2003 Diffusivities and velocity spectra of small inertial particles in turbulent-like flows. *Proc. R. Soc. Lond.* A **459**, 445–493.

Gilbertson, M. & Yates, J. 1995 The motion of particles near a bubble in a gas-fluidized bed. *J. Fluid Mech.* **323**, 377–385.

Hunt, J. & Eames, I. 2002 The disappearance of laminar and turbulent wakes in complex flows. *J. Fluid Mech.* **457**, 111–132.

Hunt, J., Perkins, R. & Fung, J. 1994 Problems in modelling disperse two-phase flows. *Appl. Mech. Rev.* **47**, S49–S60.

Launay, L., Huilier, D. & Burnage, H. 1999 Lagrangian simulation of the long time dispersion in solid–gas flows. In *3rd Intl Conf. Multiphase Flow*. Lyon.

Magnaudet, J. & Eames, I. 2000 The motion of high-Reynolds number bubbles in homogenous flows. *Annu. Rev. Fluid Mech.* **32**, 659–708.

Magnaudet, J., Rivero, M. & Fabre, J. 1987 Accelerated flows past a rigid sphere or a spherical bubble. Part 1. Steady straining flow. *J. Fluid Mech.* **284**, 97–135.

Maxey, M. 1987 The gravitation settling of aerosol particles in homogeneous turbulence and random fields. *J. Fluid Mech.* **174**, 441–465.

Milne-Thomson, L. 1968 *Theoretical Hydrodynamics*, 5th edn. Macmillan.

Pasquill, F. 1974 *Atmospheric Diffusion*, 2nd edn. John Wiley.

Roberts, E. & Mackley, M. 1996 The development of asymmetry and period doubling for oscillatory flows in baffled reactors. *J. Fluid Mech.* **328**, 19–48.

Rowe, P. 1962 The effect of bubbles on gas–solids contacting in fluidized beds. *Chem. Engng Prog. Symp.* **58**, 42–56.

Saffman, P. 1965 The lift on a small sphere in a slow shear flow. *J. Fluid Mech.* **22**, 385–400.

Soo, M. 1967 *Fluid Dynamics of Multiphase Flow Systems*. Blaisdall.

Srdic, A. 1999 Interaction of dense particles with stratified and turbulent environments. PhD thesis, Arizona State University.

Taylor, G. 1928 The energy of a body moving in an infinite fluid, with application to airships. *Proc. R. Soc. Lond.* A **70**, 13–31.

Tchen, C. 1947 Mean value and correlation problems connected with the motion of small particles suspended in a fluid. PhD thesis, Delft University of Technology.

Vincent, A. & Meneguzzi, M. 1994 The dynamics of vorticity tubes in homogeneous turbulence. *J. Fluid Mech.* **258**, 245–254.

Wells, M. & Stock, D. 1983 The effect of crossing trajectories on the dispersion of particles in a turbulent flow. *J. Fluid Mech.* **136**, 31–62.

Yih, C. 1985 New derivations of Darwin's theorem. *J. Fluid Mech.* **152**, 163–172.